Journal of Radioanalytical and Nuclear Chemistry (2024) 333:1287–1300
https://doi.org/10.1007/s10967-023-09344-y

# Prompt gamma rays of terbium induced by inelastic scattering of fission neutrons

Niklas Ophoven[1,2] · Zeljko Ilic[1,3] · Eric Mauerhofer[1] · Tsitohaina H. Randriamalala[1] · Egor Vezhlev[1] · Christian Stieghorst[4] · Zsolt Révay[4] · Jan Jolie[2] · Erik Strub[2]

Received: 10 October 2023 / Accepted: 23 December 2023 / Published online: 6 February 2024


## Abstract

Prompt gamma rays of terbium emitted after (n,n′γ) inelastic scattering reactions induced by irradiation of a terbium(III) hexahydrate ($TbCl_3 \cdot 6H_2O$) sample with a beam of fission neutrons were investigated with the instrument FaNGaS (Fast Neutron-induced Gamma-ray Spectrometry) at an angle of 90° between neutron beam and detector. At sample position, the fast-neutron flux was $1.13 \times 10^8$ cm$^{-2}$ s$^{-1}$ and the neutron beam has an average energy of 2.30 MeV. We identified 124 prompt gamma lines from the $^{159}$Tb(n,n′γ)$^{159}$Tb reaction. Presence of prompt gamma rays from oxygen and chlorine was used for a concise verification of recently published results. Relative gamma-ray intensities, effective cross sections and fast-neutron spectrum-averaged partial production cross sections of the gamma lines are given including comparisons with available literature data. We found a reasonable agreement and the multitude of unreported lines adds decisive value to nuclear spectroscopy. Additionally, we estimated the detection limit of terbium as 1 mg for a counting time of 12 h.

**Keywords** Inelastic scattering · Terbium · Chlorine · Cross section · Neutron capture · Gamma ray

## Introduction

At Heinz Maier-Leibnitz Zentrum (MLZ), Prompt Gamma Neutron Activation Analysis (PGNAA) [1–3] with cold and thermal neutrons is routinely used to determine non-destructively the elemental composition of small samples [4–8]. The FaNGaS (Fast Neutron-induced Gamma-ray Spectrometry) instrument was installed at MLZ in 2014 [9–14] and upgraded in 2020 [15, 16] to enable chemical analysis of large or small objects with fission neutrons, whose advantages were already demonstrated several decades ago [17–21]. The latter ones are produced with a converter made of uranium, which is highly-enriched (93% of $^{235}$U) and plunged into the heavy water moderator of the research reactor FRM II (Forschungs-Neutronenquelle Heinz Maier-Leibnitz). Beamtube SR10 (Strahlrohr 10) is used to extract the neutron beam from the outer core region into the experimental room of the MEDAPP (Medical Application) instrument [22] by means of various collimators and filters. The detection of the gamma radiation induced by fast-neutron interactions within the sample is performed with a high-purity germanium (HPGe) detector that is well-shielded and positioned at an angle of 90° relative to the axis of the incident neutron beam. In contrast to PGNAA, which is based on radiative neutron capture processes, prompt gammas induced by inelastic scattering of fast neutrons, i.e. (n,n′γ) reactions, are mainly measured with FaNGaS. We call this method here "Prompt Gamma Analysis based on Inelastic Neutron Scattering" (PGAINS), even if in some cases gammas from other fast-neutron reactions such as (n,pγ)- or (n,αγ)-reactions can be detected [15, 16].

The development of a comprehensive data catalogue on (n,n′γ) reactions is a primary objective of FaNGaS, aside from experimental and numerical optimization studies aiming for a higher peak-to-background ratio. Since the need for precise information on (n,n′γ) reactions is observed to be

✉ Niklas Ophoven
n.ophoven@fz-juelich.de

1 Jülich Centre for Neutron Science, Forschungszentrum Jülich GmbH, 52425 Jülich, Germany

2 Mathematisch-Naturwissenschaftliche Fakultät, Universität zu Köln, 50923 Cologne, Germany

3 Lehrstuhl Für Experimentalphysik IVc, RWTH Aachen University, 52056 Aachen, Germany

4 Heinz Maier-Leibnitz Zentrum (MLZ), Technische Universität München, Lichtenbergstraße 1, 85748 Garching, Germany

continuously increasing in both the industrial and scientific community of nuclear technology and science [23–25], the aforementioned data is expected to meet this demand. Furthermore, it complements the"Atlas of Gamma-rays from the Inelastic Scattering of Reactor Fast Neutrons", which was published by Demidov et al. in 1978 [26] and basically represents the only available database of inelastic neutron scattering. Although the data derived from measurements at FRM II generally is in reasonable agreement with the data from Demidov et al. [12–16], we pointed out the need for a cautious reevaluation of the data given in [26]. In addition, the FRM II measurements make new gamma-ray data available for the nuclear data community since they are performed with a mean energy of the incident neutron beam (2.30 MeV) that is closer to the expectation value of a classical fission spectrum on the one hand and much higher than in the work of Demidov et al. (0.63 MeV [27]) on the other hand.

In this work, nuclear data derived from the measurement of the prompt gamma rays of terbium induced by inelastic scattering of fast neutrons on a terbium(III) chloride hexahydrate ($TbCl_3 \cdot 6H_2O$) sample is presented. The thermal and epithermal neutron flux within the sample was experimentally determined in order to correct interferences from radiative capture lines. Numerical simulations of the sample flux were also performed to determine the moderation of the neutrons due to the water of crystallization and the neutron self-shielding factors as well as to investigate a possible increase of the incident thermal and epithermal neutron flux due to the installation of the new multi-leaf collimator (MLC) as presumed in our previous work [15]. We present relative intensities and fast-neutron spectrum averaged partial cross sections of the terbium gamma lines inlcuding comparisons with available literature data. Additionally, cross sections measured for the oxygen and chlorine lines are compared with the values obtained in [15, 16]. Furthermore, we give the elemental detection limit for terbium.

## Experimental

Prompt gamma radiation generated by interactions of a fission neutron beam with a $TbCl_3 \cdot 6H_2O$ powder sample (mass: 2.05 g, Tb: 0.87 g, Cl: 0.58 g, O: 0.53 g) was examined with the FaNGaS instrument. Technical specifications of the latter one can be found in [15]. During measurement, the powder was contained in a small bag of PTFE (Polytetrafluorethylene), whose maximum thickness was estimated as 6 mm. Attached to a thin PTFE rod, the sample was tilted by an angle of 45° with respect to the incident beam direction. In front of the sample, the magnitude of the fast-neutron flux was $(1.13 \pm 0.04) \times 10^8$ cm$^{-2}$ s$^{-1}$ with an average neutron energy of 2.30 MeV. The sample was irradiated for 9.7 h and counted for 7.7 h (live time). The gamma rays were measured at a sample-to-detector distance of 67 cm and perpendicular to the neutron beam direction, i.e. at an angle of 90°. The analysis of the recorded spectrum was carried out using the HYPERMET-PC software [28] and it is depicted in Figs. 1 and 2. Prompt gamma rays associated to fast-neutron reactions were identified using the NuDat 3.0 database [29] as well as related nuclear data from different evaluations for all nuclides covered in this work [30–33]. Gamma rays from radiative capture reactions were identified with the PGNAA database [34].

Since a small fraction of neutrons scatter towards the detector the count rate of background lines was found to be increased by a mean factor of $1.53 \pm 0.32$. This factor was used in the interference corrections of background lines. Relevant interferences arising from escape peaks (denoted as SE and DE for a single or double escape peak, respectively) were found for two lines and corrected with the correction curves given in [16].

## Method

For a prompt gamma ray of energy $E_\gamma$ and produced by neutron capture or inelastic neutron scattering the net peak area, i.e. $P_{E\gamma}$, can be described as [1, 12–16]:

$$P_{E\gamma} = \frac{m}{M} \cdot N_A \cdot h \cdot \varepsilon_{E\gamma} \cdot \langle \sigma_{E\gamma} \rangle \cdot \langle \Phi \rangle \cdot t_c \cdot f_n \cdot f_{mod} \cdot f_{E\gamma} \quad (1)$$

where $m$ ($g$) represents the mass of the considered element, $M$ ($g$ mol$^{-1}$) equals the molar mass of the element, $N_A$ is the Avogadro number, $h$ the abundance of the considered isotope, $\varepsilon_{E\gamma}$ the full-energy-peak (FEP) efficiency, $<\sigma_{E\gamma}>$ (cm$^2$) the spectrum-averaged isotopic cross section for gamma-ray production, $<\Phi>$ (cm$^{-2}$ s$^{-1}$) the integral neutron flux in the considered energy range, $t_c$ ($s$) the counting live time, $f_n$ the neutron self-shielding factor and $f_{E\gamma}$ the gamma-ray self-absorption factor. The factor $f_{mod}$ accounts for possible moderation effects in samples that contain water.

The gamma-ray self-absorption factor $f_{E\gamma}$ was calculated analytically according to the following equation [1, 35]:

$$f_{E\gamma} = \frac{1 - e^{-\frac{\mu}{\rho} \cdot \rho \cdot l}}{\frac{\mu}{\rho} \cdot \rho \cdot l} \quad (2)$$

where $l = 0.85$ cm is the effective thickness of the sample, $\mu/\rho$ (cm$^2$ g$^{-1}$) represents the mass attenuation coefficient and $\rho = 4.35$ g cm$^{-3}$ is the sample density. Including coherent scattering, the value of $\mu/\rho$ was obtained from the NIST (National Institute of Standards and Technology) photon cross sections database XCOM [36, 37]. For several discrete energies ranging between 100 and 5000 keV the corresponding $f_{E\gamma}$ values were calculated using Eq. (2). The variation

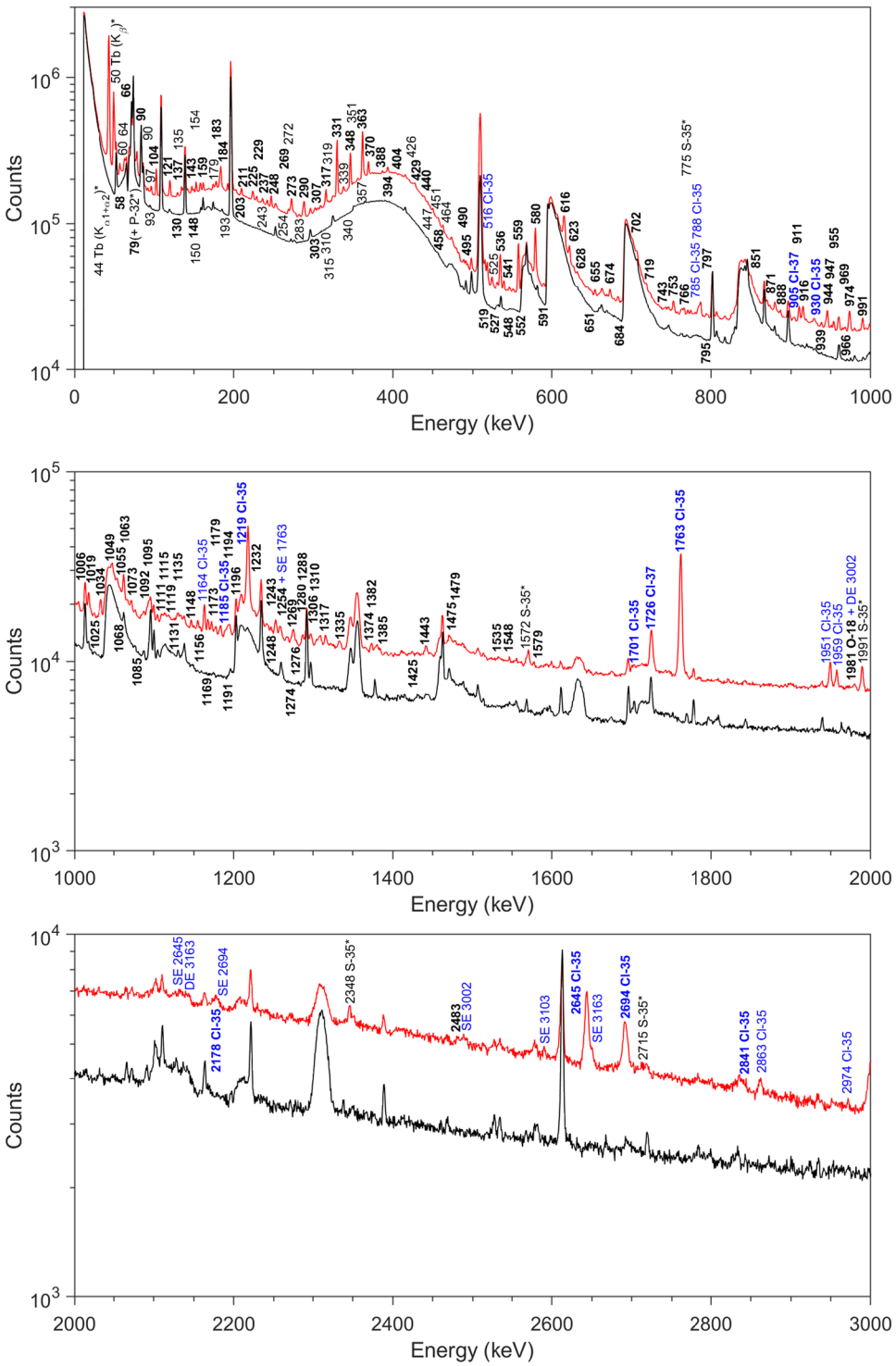


**Fig. 1** Measured gamma-ray spectra in the energy range from 0 to 3000 keV. The spectrum of the $TbCl_3{\cdot}6H_2O$ sample (red) was obtained during 27,879 s counting live time and the spectrum of the beam background (black) during 51,506 s. Prompt gamma rays that are written in black with an asterisk belong to either (n,pγ) reactions (S-35) and (n,αγ) reactions (P-32) on Cl-35 or represent X-rays from terbium. Prompt gamma rays marked in black and bold are issued from (n,n′γ) inelastic scattering of fast neutrons on terbium. Prompt gamma rays from (n,γ) radiative capture reactions in terbium are written in black. Gamma rays written in bold blue are induced by inelastic scattering reactions on chlorine. Radiative capture gamma rays from Cl-35 are marked with light blue. Single and double escape peaks are indicated by the abbreviations SE and DE, respectively. Our former publications [10, 12] provide information on the origin of relevant background lines

of the gamma-ray self-absorption factors $f_{E\gamma}$ as a function of the gamma-ray energy $E_\gamma$ is depicted in Fig. 3. Individual data points were fitted with a semi-empirical function that is given as:

$$f = a_0 + a_1 \cdot \left(1 - e^{-a_2 \cdot E_\gamma}\right) + a_3 \cdot \left(1 - e^{-a_4 \cdot E_\gamma}\right) \quad (3)$$

with $a_0 = -0.8829 \pm 0.0528$, $a_1 = 0.1558 \pm 0.0187$, $a_2 = 0.0011 \pm 0.0002$, $a_3 = 1.6665 \pm 0.0416$ and $a_4 = 0.0098 \pm 0.0004$.

The value of $<\sigma_{E\gamma}>$ in Eq. (1) is coupled with the effective cross section $<\sigma>$ ($cm^2$) of a certain reaction via the absolute gamma-ray intensity $I_{E\gamma}$, including the contribution of internal conversion, as:

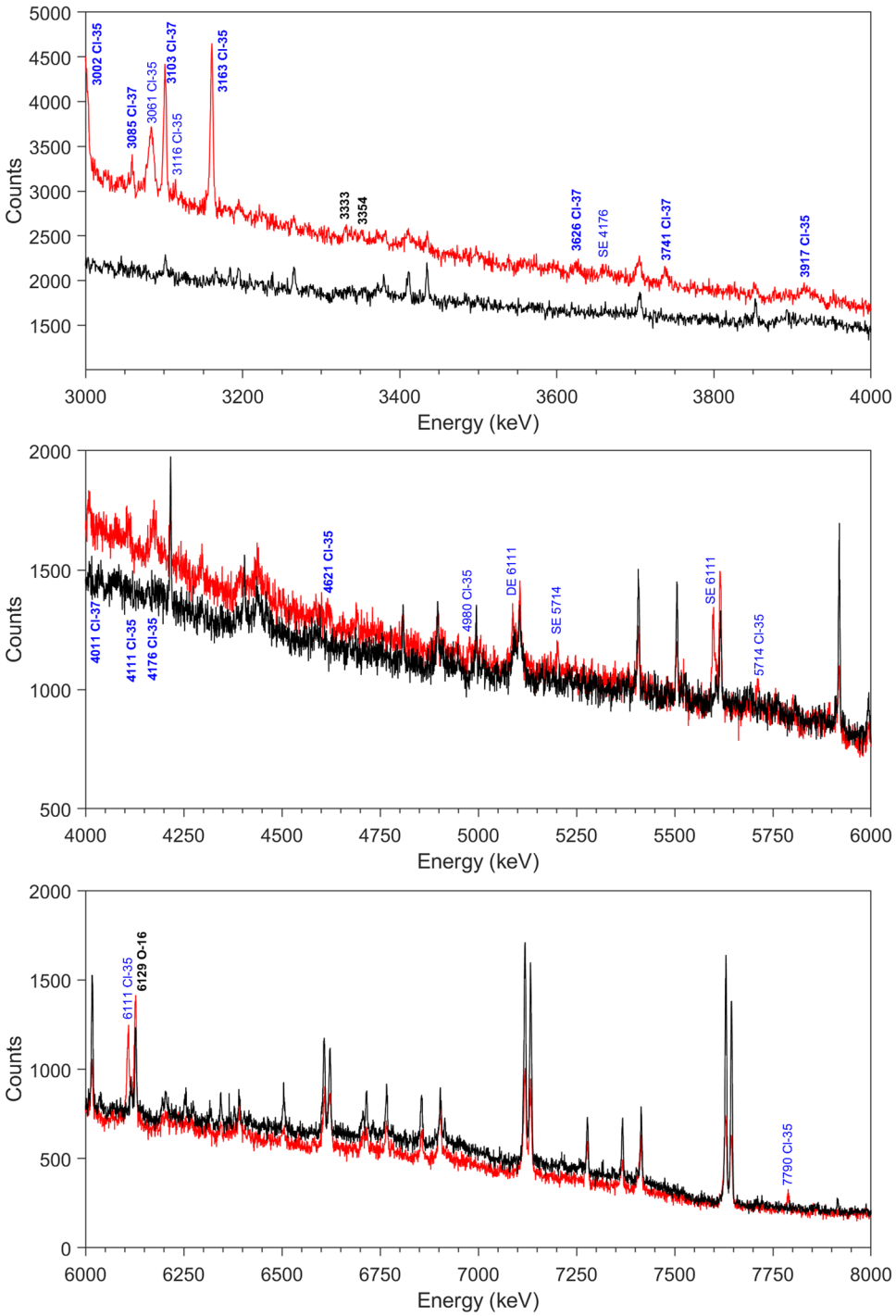


**Fig. 2** Measured gamma-ray spectra in the energy range from 3000 to 8000 keV. The spectrum of the $TbCl_3{\cdot}6H_2O$ sample (red) was obtained during 27,879 s counting live time and the spectrum of the beam background (black) during 51,506 s. Prompt gamma rays marked in black and bold are issued from (n,n′γ) inelastic scattering of fast neutrons on terbium. Gamma rays written in bold blue are induced by inelastic scattering reactions on chlorine. Radiative capture gamma rays from Cl-35 are marked with light blue. Single and double escape peaks are indicated by the abbreviations SE and DE, respectively. Our former publications [10–12] provide information on the origin of relevant background lines

$$\langle \sigma_{E\gamma} \rangle = I_{E\gamma} \cdot \langle \sigma \rangle \tag{4}$$

The effective cross section $<\sigma>$ can be expressed as follows:

$$\langle \sigma \rangle = \frac{\sum_{i=m}^{n} \sigma(E_i) \bullet \Phi(E_i)}{\sum_{i=m}^{n} \Phi(E_i)} \tag{5}$$

where $\Phi(E_i)$ denotes the neutron flux in the neutron energy bin $i$ and $\sigma(E_i)$ the neutron-bin averaged reaction cross section. The value of $i=m$ corresponds to the first and $i=n$ to the last neutron-energy bin in the considered neutron-energy ranges. The term $\sum_{i=m}^{n} \sigma(E_i) \bullet \Phi(E_i)$ gives the rate of the reaction in units of $atom^{-1}\ s^{-1}$.

With respect to the irradiation geometry of the previous FaNGaS set-up [12] we showed in [15] that the

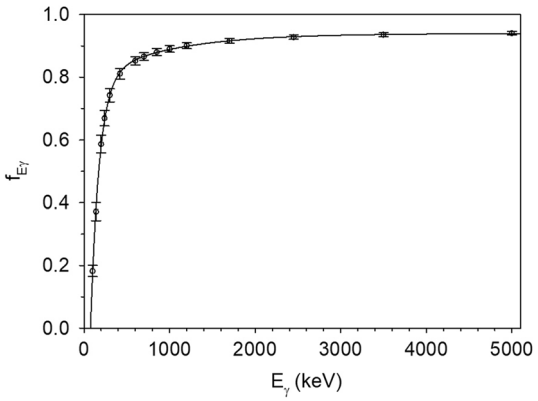


**Fig. 3** Variation of the gamma-ray self-absorption factor $f_{E\gamma}$ as a function of the gamma-ray energy $E_\gamma$. The data points were obtained from NIST XCOM [36, 37] and the fit of the data after Eq. (3) is shown by the solid line

fast-neutron flux at irradiation position was reduced by about 20% due to an increase of the sample-to-neutron-source distance related to the installation of the new MLC of the MEDAPP facility. The same reduction is simply assumed here for the thermal and epithermal neutron flux and the resulting neutron energy spectrum at sample position is shown in Fig. 4. It can be split into three energy ranges designated as thermal ($10^{-10}$ MeV $< E_i <$ $1.42 \times 10^{-7}$ MeV, $m = 1$, $n = 7$), epithermal ($1.42 \times 10^{-7}$ MeV $< E_i <$ 0.06 MeV, $m = 8$, $n = 49$) and fast (0.06 MeV $< E_i <$ 20 MeV, $m = 50$, $n = 100$), with the respective neutron fluxes of $(7.63 \pm 2.27) \times 10^2$ cm$^{-2}$ s$^{-1}$, $(1.50 \pm 0.07) \times 10^6$ cm$^{-2}$ s$^{-1}$ and $(1.13 \pm 0.04) \times 10^8$ cm$^{-2}$ s$^{-1}$. The integral neutron flux, covering all three aforementioned energy regions, is $(1.15 \pm 0.04) \times 10^8$ cm$^{-2}$ s$^{-1}$. The values of $\sigma(E_i)$ were produced with the RECONR, BROADR and GROUPR modules of the NJOY Nuclear Data Processing System (Version 2016) [38, 39] using ENDF/B-VIII.0 [40] nuclear data library for the $^{35}$Cl(n,n′γ)$^{35}$Cl, $^{35}$Cl(n,pγ)$^{35}$S, $^{35}$Cl(n,αγ)$^{32}$P, $^{37}$Cl(n,n′γ)$^{37}$Cl, $^{159}$Tb(n,γ)$^{160}$Tb and $^{159}$Tb(n,n′γ)$^{159}$Tb reactions. In the case of $^{35}$Cl(n,γ)$^{36}$Cl, the nuclear data from ENDF-B-VIII.0 [40], JENDL4.0 [41], JEFF-3.3 [42] and TENDL-2019 [43] were considered due to considerable deviations between these libraries.

The effective cross sections $<\sigma>$ determined by means of Eqs. (4) and (5), respectively, are given in Table 1 for the aforementioned neutron-energy ranges and observed reactions. The neutron-energy dependence of the NJOY grouped cross sections is depicted along with the neutron energy spectrum in Fig. 4. Due to large uncertainties of the flux in the thermal neutron-energy range, cross sections given in JANIS (Java-based nuclear information software) [44] were preferred.

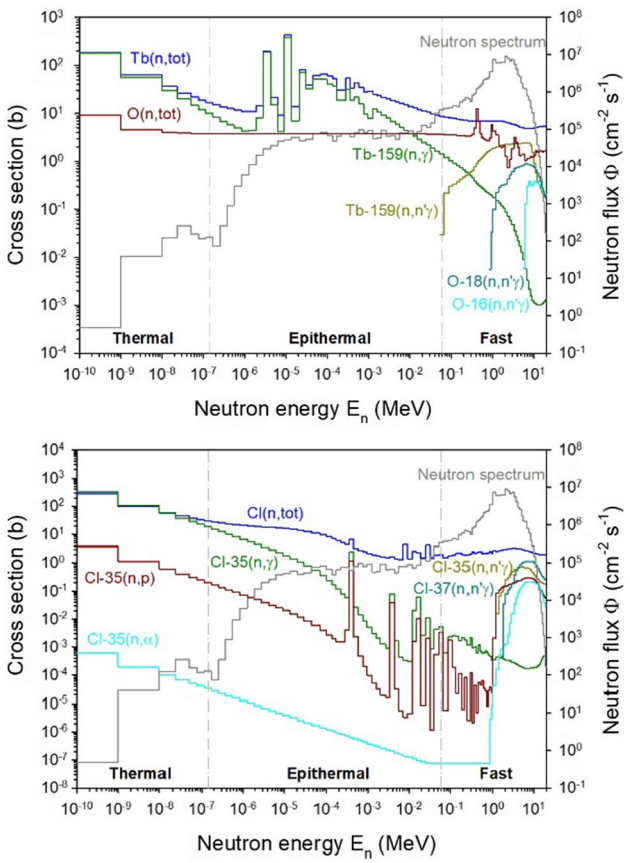


**Fig. 4** Neutron energy spectrum of FaNGaS as assumed in [15, 16] incident on the sample (right scale of *y*-axis) and variation of the NJOY grouped microscopic cross sections $\sigma_i(E)$ averaged over the neutron energy bin *i* as a function of the neutron energy (left scale of *y*-axis) for total (n,tot), fast-neutron inelastic scattering (n,n′γ), (n,pγ) and (n,αγ) reactions for terbium and oxygen (top side) and chlorine (bottom side). The values of the (n,tot) reaction for oxygen and chlorine are elemental and they were calculated as the sum of isotopic cross sections in each energy bin multiplied with the corresponding isotopic abundance

## Sample neutron flux

Many radiative-capture lines of $^{159}$Tb were found to interfere with lines from the $^{159}$Tb(n,n′γ)$^{159}$Tb reaction and their corrections require knowledge on the thermal and epithermal neutron flux within the sample. The latter contains 29 wt% water of crystallization, which could moderate the epithermal neutrons of the incident beam.

The sample neutron flux was determined in a first step by means of numerical simulation performed with the Monte Carlo N-Particle (MCNP, version 6.1) [45, 46] code. Use of ENDF/B-VIII.0 data [40] was enabled by means of the Lib80x library [47]. The neutron-energy distribution of the incident spectrum given in Fig. 4 was used to simulate the irradiation of a 6 mm thick $TbCl_3 \cdot 6H_2O$ slab with a mass corresponding to the one of our experiment and tilted by

**Table 1** Effective cross sections $<\sigma>$ for (n,γ), (n,n′γ), (n,pγ) and (n,αγ) reactions observed from the irradiation of the $TbCl_3{\cdot}6H_2O$ sample calculated with Eq. (5) and neutron self-shielding factors $f_n$ for all three neutron-energy ranges considered determined with MCNP6 [45, 46]. Data for the total (n,tot) reaction is given elementary

| Neutron-energy range | $10^{-10}$–$1.4{\cdot}10^{-7}$ MeV (thermal) | | $1.4{\cdot}10^{-7}$–0.06 MeV (epithermal) | 0.06–20 MeV (fast) |
|---|---|---|---|---|
| Cross sections | $<\sigma$th$>$ (b) | $<\sigma$th$>$ (b)[a] | $<\sigma_{epi}>$ (*b*) | $<\sigma_{fast}>$ (mb) |
| $^{16}O(n,n'\gamma)^{16}O$ | – | – | – | 8.49(72) |
| $^{18}O(n,n'\gamma)^{18}O$ | – | – | – | 347(32) |
| O(n,tot) | 3.93(188) | 4.45(4) | 3.76(66) | 2562(314) |
| $^{35}Cl(n,\gamma)^{36}Cl$ | 38.035(1) | 43.61(1) | 0.37(1) | 0.72(19) |
| $^{35}Cl(n,n'\gamma)^{36}Cl$ | – | – | – | 238(21) |
| $^{35}Cl(n,p)^{35}S$ | 0.437(216) | 0.485(6) | 0.029(5) | 119(11) |
| $^{35}Cl(n,\alpha)^{32}P$ | 0.07(4)[b] | 0.0801(1)[b] | $8.69(121){\cdot}10^{-4}$[b] | 22(1) |
| $^{37}Cl(n,n'\gamma)^{38}Cl$ | – | – | – | 177 (15) |
| Cl(n,tot) | 46.76(2266) | 51.73(4) | 4.75(63) | 2840(245) |
| $^{159}Tb(n,\gamma)^{160}Tb$ | 20.41(990) | 23.37(24) | 20.63(287) | 146(20) |
| $^{159}Tb(n,n'\gamma)^{159}Tb$ | – | – | – | 1974(206) |
| Tb(n,tot) | 28.27(1384) | 31.21(26) | 32.46(484) | 6490(733) |
| $f_n$ | 0.772 | | 0.976 | 0.991 |

a: mean value of cross sections from various data libraries provided in JANIS [44]. b: mb.

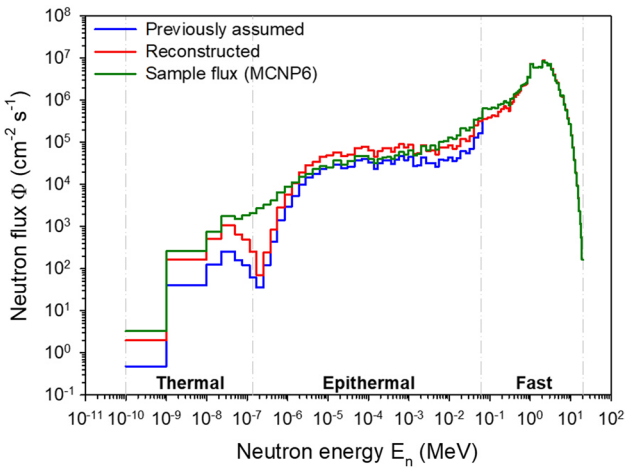


**Fig. 5** Neutron energy spectrum of FaNGaS assumed in our previous works [15, 16] (blue curve), reconstructed in this work (red) and the volume-averaged sample flux derived with MCNP6 (dark green)

an angle of 45°. The sample neutron flux, derived with the F4 Tally, is depicted in Fig. 5. It shows a non-negligible increase of the flux below a neutron energy of 1 eV resulting from water moderation. The flux in the three neutron energy regions is $(8.3 \pm 2.5) \times 10^3$ cm$^{-2}$ s$^{-1}$ for thermal neutrons, $(3.2 \pm 0.4) \times 10^6$ cm$^{-2}$ s$^{-1}$ for epithermal neutrons and $(1.15 \pm 0.09) \times 10^8$ cm$^{-2}$ s$^{-1}$ for fast neutrons. In order to determine the neutron self-shielding ($f_n$), irradiation of the sample with each component of the incident flux (thermal, epithermal and fast) was simulated separately with $10^8$ primary neutrons. The neutron self-shielding factor was calculated as the ratio of the neutron flux within the sample (F4 tally) to the neutron flux within a diluted sample of $10^{-6}$ the density [48–50], i.e. in void in practice. In fact, this is equivalent to the ratio of the sample flux (F4 tally) to the incident neutron flux (F2 tally). The value of $f_n = 0.991$ for fast neutrons implies that the self-shielding effect is negligible, whereas values of $f_n = 0.772$ for thermal and $f_n = 0.976$ for epithermal neutrons must be considered. The simulations to determine the moderation ($f_{mod}$) factors comprised also three simulations (thermal, epithermal, integral) and the number of primary particles was chosen here to yield statistical uncertainties of the same order of magnitude in each simulation. The moderation factors were calculated as the ratio of the thermal and epithermal sample neutron flux obtained from the simulations with the part of the incident neutron-energy distribution of interest (i.e. thermal and epithermal) to the simulation with the whole incident neutron-energy distribution (flux values given above). The resulting moderation factors are $f_{mod} = 14 \pm 6$ for thermal neutrons and $f_{mod} = 2.1 \pm 0.4$ for epithermal neutrons. Dividing the sample fluxes by the corresponding shielding and moderation factors reproduces well the incident flux values at sample position as given above.

The thermal and epithermal neutron flux within the sample were also determined experimentally from the net counts of the interference-free capture lines of $^{159}$Tb (193, 243, 339, 357, 451, 464 and 525 keV) and $^{35}$Cl (1164, 1951 and 1959 keV) using Eq. (1) with $f_n = 1$ and $f_{mod} = 1$ and Eqs. (4) and (5). The intensities of the gamma rays $I_\gamma$ were deduced from the partial elemental capture cross sections and the associated isotopic cross sections for thermal neutrons as given in [34]. The counts of the $^{159}$Tb and $^{35}$Cl lines were corrected first for the contribution of the fast neutrons with a flux of $1.13 \times 10^8$ cm$^{-2}$ s$^{-1}$ and the cross sections given in column 5 of Table 1. The epithermal neutron flux

was then determined directly from the lines of $^{159}$Tb as the rate of the $^{159}$Tb(n,γ)$^{160}$Tb reaction induced by thermal neutrons is negligible (the effective cross sections for thermal and epithermal neutrons are approximately the same (see Table 1) and the thermal neutron flux is about four orders of magnitude less than the epithermal neutron flux). The value obtained for the latter is $(6.1 \pm 1.6) \times 10^6$ cm$^{-2}$ s$^{-1}$. The thermal neutron flux, obtained from the lines of $^{35}$Cl after correction of the contribution of epithermal neutrons, is $(3.4 \pm 1.4) \times 10^4$ cm$^{-2}$ s$^{-1}$. The experimentally determined sample fluxes are significantly higher than the values obtained by simulation, indicating a possible increase of the incident thermal and epithermal neutron flux owing to the MLC. Correcting the experimental flux with the corresponding shielding and moderation factors provides a thermal and epithermal flux of $(3.2 \pm 1.3) \times 10^3$ cm$^{-2}$ s$^{-1}$ and $(2.9 \pm 0.8) \times 10^6$ cm$^{-2}$ s$^{-1}$, respectively, at sample position. The ratio of these flux values to the previously assumed values yields scaling factors of $4.1 \pm 2.1$ and $2.0 \pm 0.5$, respectively, which are used to rescale the flux in each energy bin of the thermal and epithermal region, respectively. The proposed new neutron energy spectrum at sample position is shown in Fig. 5.

## Gamma rays from inelastic neutron scattering in terbium

A total of 124 prompt gamma lines assigned to the $^{159}$Tb(n,n′γ)$^{159}$Tb reaction were measured. Aforementioned gamma rays are marked accordingly in Figs. 1 and 2 and their corresponding data is provided in Table 2. Interferences with lines arising from the $^{159}$Tb(n,γ)$^{160}$Tb and $^{35}$Cl(n,γ)$^{36}$Cl reaction are corrected with the intensities taken from [34] by means of Eqs. (1), (4) and (5). Four lines were corrected for the contribution of delayed lines of $^{160}$Tb as described in [13] with intensities taken from [52]. With respect to [34] and [52] 23 radiative capture lines from $^{159}$Tb and 5 lines from $^{35}$Cl were found to interfere significantly with (n,n′γ) lines with contributions ranging between 2 and 53%. Doppler broadening [53, 54] was only observed for gamma lines from chlorine. The composition of the $TbCl_3 \cdot 6H_2O$ sample was checked using the measurement of the PVC foil performed in our previous work on $CeCl_3$ [16]. The interference-free (with respect to data on [29, 30]) lines at 1185, 1763, 2645, 2694, 3002, 3085, 3103 and 3163 keV (see Figs. 1 and 2) from chlorine were used to calculate an average chlorine mass of $(0.58 \pm 0.01)$ g, which agrees well with the value from the stoichiometry of the sample.

Gamma-ray intensities were determined relative to the 331-keV line. They are presented together with the values determined in [26] in columns 3 and 6 of Table 2. We have detected 54 of the 60 lines listed in the Demidov Atlas. The lines listed at energies of 154.0, 194.1, 272.9, 282.7, 339.2, 451.3, and 464.6 keV are either partly unassigned or partly assigned to radiative capture lines of $^{159}$Tb. Based on [34] we found that all of those lines belong to the neutron capture reaction in terbium except the 272.9-keV line, which belongs to the $^{159}$Tb(n,n′γ)$^{159}$Tb reaction as specified in [29, 30]. Gamma rays with energies of 260.9, 274.8, 596.4, 608.2, 617.5 and 1003.0 keV given in [26] have not been observed in our work. From the aforementioned lines, only the lines at 274.8 and 617.5 keV were assigned to fast-neutron inelastic scattering by Demidov. These assignments seem to be reasonable with respect to [29, 30], but it is surprising that our spectrometer with a better energy resolution did not distinguish the 617.5-keV line from a close-lying line at 615.4 [26], also observed in our spectrum. However, a relative intensity of $(36 \pm 2)$% for our line at 615.6 keV agrees well with the sum of the intensities of the two lines given in [26], $(34 \pm 10)$%. For the lines at 596.4 and 608.2 keV, assigned to (n,γ) reaction and unassigned, respectively, in [26], no suitable transition is proposed in [30]. In our measurement these lines are interfered by background lines of $^{74}$Ge and $^{73}$Ge [10, 12], respectively. As both lines also appear in the background analysis in the Demidov Atlas we assume an erroneous identification. Absence of the unassigned lines at 260.9 and 1003.0 keV in our measurement and missing data on [29, 30] helps providing support that they do not belong to terbium.

On the other hand, compared to [26] we have identified 76 new gamma lines. The identification of new lines is mainly associated to the better energy resolution of our spectrometer and our higher mean neutron energy (2.30 MeV vs. 0.63 MeV [27]). In contrast to [26] we were able to resolve doublets in the lines listed at energies of 184.2, 305.2, 947.0, 1094.1, 1195.1 and 1276.7 keV in [26]. It is worth to mention that from all 124 observed gamma lines 76 are not specified in [29, 30]. Of those, 16 are listed in the Demidov Atlas, confirming that they originate from fast-neutron inelastic scattering. The other 60 lines detected in our measurement are unambiguously associated to the $^{159}$Tb(n,n′γ)$^{159}$Tb reaction. All these new lines may help to extend the decay scheme of terbium.

The relationship between the relative intensities derived from our work and those listed in [26] is shown in Fig. 6. The values have been fitted with the following semi-empirical function:

$$I_R = a \cdot \left(I_{RD}\right)^b \tag{6}$$

with $a = 1.27 \pm 0.17$ and $b = 0.92 \pm 0.06$.

The two measurements show a good agreement as the average value of the intensity ratio, i.e. $I_R/I_{RD}$, is $1.16 \pm 0.39$. In order to assess the consistency further, the two data sets are shown in Fig. 7 as a histogram of the residuals $R$ in units of standard deviation [$\sigma$], determined as:

**Table 2** Prompt gamma rays of $^{159}$Tb[a] induced by inelastic scattering of fast neutrons

| This work | | | | From Demidov Atlas [26] | | *R* |
|---|---|---|---|---|---|---|
| $E_\gamma$ (keV) | $P_{E\gamma}(90°)/(\varepsilon_{E\gamma}.f_{E\gamma})\times10^{-8}$ (count) | $I_R$(relative) (%) | $<\sigma_{E\gamma}(90°)>$ (mb) | $E_\gamma$ (keV) | $I_R$(relative) (%) | |
| 57.92 ± 0.06 | 46 ± 6 | 156 ± 19 | 445 ± 63 | – | – | – |
| 66.27 ± 0.08[b] | 2.07 ± 0.53 | 7.00 ± 1.81 | 19.9 ± 5.4 | – | – | – |
| 79.29 ± 0.07[c,d] | 41 ± 6 | 140 ± 20 | 397 ± 63 | – | – | – |
| 90.29 ± 0.08[d] | 3.09 ± 0.49 | 10.4 ± 1.7 | 30 ± 5 | – | – | – |
| 103.71 ± 0.03[d] | 22 ± 1 | 75 ± 3 | 214 ± 18 | – | – | – |
| 120.74 ± 0.03 | 8.61 ± 0.61 | 29 ± 2 | 83 ± 9 | 121.3 ± 0.4 | 16 ± 5 | 2.38 |
| 130.31 ± 0.07[d] | 0.32 ± 0.05 | 1.07 ± 0.16 | 3.04 ± 0.52 | – | – | – |
| 137.39 ± 0.04 | 2.87 ± 0.13 | 9.67 ± 0.53 | 28 ± 2 | 137.1 ± 0.6 | 6.0 ± 1.5 | 2.31 |
| 142.83 ± 0.09 | 1.90 ± 0.16 | 6.42 ± 0.59 | 18.3 ± 2.1 | – | – | – |
| 148.26 ± 0.04 | 2.72 ± 0.11 | 9.18 ± 0.47 | 26 ± 2 | 149.0 | 6.0 ± 1.0 | 2.88 |
| 158.95 ± 0.05[b] | 2.32 ± 0.38 | 7.84 ± 1.30 | 22 ± 4 | 159.0 ± 0.4 | 4.0 ± 0.8 | 0.15 |
| 183.06 ± 0.07[d] | 3.77 ± 0.30 | 12.7 ± 1.1 | 36 ± 4 | – | – | – |
| 184.48 ± 0.05[d] | 8.00 ± 0.68 | 27 ± 2 | 77 ± 9 | 184.2 ± 0.3[e] | 30 ± 3 | 3.23 |
| **203.50 ± 0.09**[d,f] | 1.34 ± 0.15 | 4.51 ± 0.53 | 12.8 ± 1.8 | – | – | – |
| 210.53 ± 0.04[d] | 2.34 ± 0.13 | 7.89 ± 0.49 | 22 ± 2 | 210.7 ± 0.6 | 4.5 ± 0.7 | 3.96 |
| 224.67 ± 0.08 | 3.28 ± 0.19 | 11.1 ± 0.7 | 31 ± 3 | 224.5 ± 0.6 | 7.2 ± 2.0 | 1.82 |
| 229.38 ± 0.05[d] | 1.40 ± 0.09 | 4.73 ± 0.34 | 13.5 ± 1.4 | 228.2 ± 0.8 | 2.5 ± 1.2 | 1.79 |
| 237.00 ± 0.05[d] | 1.41 ± 0.09 | 4.75 ± 0.33 | 13.5 ± 1.4 | 237.2 ± 0.4 | 2.7 ± 0.5 | 3.42 |
| 247.67 ± 0.04[d] | 1.55 ± 0.20 | 5.23 ± 0.69 | 14.9 ± 2.2 | 247.6 ± 0.4 | 3.2 ± 0.5 | 2.38 |
| 269.31 ± 0.07[d] | 0.93 ± 0.11 | 3.14 ± 0.39 | 8.95 ± 1.29 | 269.1 ± 0.8 | 1.8 ± 0.7 | 1.67 |
| 273.30 ± 0.05[d] | 4.30 ± 0.32 | 14.5 ± 1.2 | 41 ± 4 | 272.9 ± 0.6[g] | 13 ± 3 | 0.47 |
| 289.77 ± 0.09[d] | 5.01 ± 0.25 | 16.9 ± 1.0 | 48 ± 4 | 289.6 | 16 ± 2 | 0.41 |
| 303.40 ± 0.09[d] | 0.76 ± 0.11 | 2.57 ± 0.39 | 7.31 ± 1.23 | – | – | – |
| 306.82 ± 0.11[d] | 0.75 ± 0.13 | 2.53 ± 0.43 | 7.21 ± 1.33 | 305.2 ± 0.6[e] | 6.3 ± 1.0 | − 1.03 |
| 317.01 ± 0.05[d] | 3.56 ± 0.33 | 12.0 ± 1.2 | 34 ± 4 | 317.4 ± 0.3 | 13.1 ± 1.5 | − 0.58 |
| 330.89 ± 0.03 | 30 ± 1 | 100.0 | 285 ± 24 | 331.4 ± 0.3 | 100.0 | – |
| 347.61 ± 0.03[d] | 18.1 ± 0.6 | 61 ± 3 | 174 ± 15 | 348.3 ± 0.3 | 65 ± 5 | − 0.68 |
| 362.89 ± 0.07[d] | 31 ± 1 | 106 ± 5 | 302 ± 25 | 363.5 ± 0.3 | 100 ± 7 | 0.70 |
| 370.16 ± 0.03[d] | 6.96 ± 0.26 | 23 ± 1 | 67 ± 6 | 370.7 ± 0.3 | 21 ± 2 | 1.07 |
| 387.74 ± 0.07 | 1.36 ± 0.15 | 4.58 ± 0.51 | 13.0 ± 1.7 | 388.3 ± 0.6 | 6.3 ± 0.8 | − 1.81 |
| 394.41 ± 0.04 | 3.17 ± 0.18 | 10.7 ± 0.7 | 30 ± 3 | 395.1 ± 0.4 | 13 ± 2 | − 1.09 |
| **404.26 ± 0.21**[f] | 0.41 ± 0.10 | 1.39 ± 0.35 | 3.96 ± 1.04 | 402.6 ± 0.6 | 6.4 ± 1.2 | − 4.00 |
| 428.54 ± 0.09[d] | 1.68 ± 0.16 | 5.67 ± 0.56 | 16.1 ± 2.0 | 429.1 ± 0.6 | 6.9 ± 1.0 | − 1.07 |
| 440.26 ± 0.10 | 1.43 ± 0.15 | 4.81 ± 0.53 | 13.7 ± 1.8 | – | – | – |
| **457.78 ± 0.13**[f] | 1.28 ± 0.13 | 4.33 ± 0.45 | 12.3 ± 1.5 | 457.7 ± 0.7 | 3.1 ± 0.7 | 1.49 |
| **489.71 ± 0.17**[f] | 0.67 ± 0.12 | 2.25 ± 0.42 | 6.40 ± 1.28 | – | – | – |
| 494.56 ± 0.18 | 0.55 ± 0.11 | 1.87 ± 0.38 | 5.32 ± 1.13 | – | – | – |
| 519.24 ± 0.06[d] | 1.45 ± 0.18 | 4.88 ± 0.61 | 13.9 ± 2.0 | 520.1 ± 0.6 | 5.8 ± 0.8 | − 0.91 |
| **526.90 ± 0.19**[f] | 0.27 ± 0.05 | 0.90 ± 0.17 | 2.56 ± 0.50 | – | – | – |
| 536.14 ± 0.04 | 3.81 ± 0.23 | 12.9 ± 0.9 | 37 ± 4 | 536.8 ± 0.3 | 15 ± 2 | − 0.98 |
| 540.62 ± 0.06 | 1.04 ± 0.08 | 3.50 ± 0.30 | 9.98 ± 1.12 | 541.7 ± 0.8 | 3.0 ± 0.6 | 0.75 |
| **547.75 ± 0.14**[f] | 0.42 ± 0.06 | 1.43 ± 0.21 | 4.07 ± 0.67 | – | – | – |
| **552.38 ± 0.20**[f] | 0.30 ± 0.06 | 1.01 ± 0.21 | 2.88 ± 0.62 | – | – | – |
| 558.76 ± 0.06 | 6.95 ± 0.21 | 23 ± 1 | 67 ± 6 | 559.6 ± 0.3 | 28 ± 4 | − 1.10 |
| 580.02 ± 0.05 | 10.1 ± 0.3 | 34 ± 2 | 97 ± 8 | 580.9 ± 0.2 | 34 ± 4 | 0.01 |
| **590.52 ± 0.12**[f] | 0.43 ± 0.05 | 1.45 ± 0.19 | 4.13 ± 0.60 | – | – | – |
| 615.58 ± 0.06 | 10.6 ± 0.3 | 36 ± 2 | 102 ± 9 | 615.4 ± 0.6[h] | 34 ± 10 | 0.17 |

**Table 2** (continued)

| This work | | | | From Demidov Atlas [26] | | *R* |
|---|---|---|---|---|---|---|
| $E_\gamma$ (keV) | $P_{E\gamma}(90°)/(\varepsilon_{E\gamma}\cdot f_{E\gamma})\times 10^{-8}$ (count) | $I_R$(relative) (%) | $<\sigma_{E\gamma}(90°)>$ (mb) | $E_\gamma$ (keV) | $I_R$(relative) (%) | |
| 622.82 ± 0.04 | 2.90 ± 0.13 | 9.79 ± 0.55 | 28 ± 3 | 623.5 ± 0.6 | 5.5 ± 0.8 | 4.43 |
| **628.20 ± 0.13**[f] | 0.55 ± 0.09 | 1.85 ± 0.30 | 5.28 ± 0.95 | – | – | – |
| **650.78 ± 0.15**[f,i] | 0.17 ± 0.04 | 0.58 ± 0.14 | 1.64 ± 0.41 | – | – | – |
| **655.02 ± 0.11**[d,f] | 0.79 ± 0.07 | 2.67 ± 0.27 | 7.60 ± 0.93 | – | – | – |
| 673.78 ± 0.10 | 1.06 ± 0.08 | 3.57 ± 0.30 | 10.2 ± 1.1 | 674.5 ± 0.7 | 3.3 ± 0.8 | −0.26 |
| 683.79 ± 0.14 | 0.79 ± 0.06 | 2.65 ± 0.22 | 7.55 ± 0.83 | – | – | – |
| 702.29 ± 0.13 | 0.69 ± 0.10 | 2.31 ± 0.34 | 6.59 ± 1.08 | – | – | – |
| **719.43 ± 0.18**[f] | 0.68 ± 0.11 | 2.28 ± 0.38 | 6.49 ± 1.18 | 718.7 ± 0.9 | 2.1 ± 0.7 | 0.23 |
| **743.07 ± 0.18**[f] | 0.39 ± 0.06 | 1.32 ± 0.19 | 3.76 ± 0.62 | – | – | – |
| 753.24 ± 0.08 | 1.46 ± 0.11 | 4.94 ± 0.39 | 14.1 ± 1.5 | 753.8 ± 0.7 | 3.2 ± 0.6 | 2.42 |
| **766.45 ± 0.09**[f] | 0.58 ± 0.05 | 1.96 ± 0.19 | 5.57 ± 0.66 | 765.3 ± 0.9 | 1.7 ± 0.6 | 0.41 |
| **794.81 ± 0.13**[f] | 0.39 ± 0.05 | 1.31 ± 0.16 | 3.72 ± 0.52 | – | – | – |
| **796.86 ± 0.17**[f] | 0.28 ± 0.04 | 0.96 ± 0.15 | 2.72 ± 0.47 | – | – | – |
| 851.05 ± 0.15 | 0.58 ± 0.12 | 1.96 ± 0.41 | 5.58 ± 1.23 | – | – | – |
| **870.97 ± 0.08**[f] | 0.82 ± 0.10 | 2.76 ± 0.35 | 7.86 ± 1.13 | – | – | – |
| **887.66 ± 0.11**[f] | 0.64 ± 0.05 | 2.16 ± 0.20 | 6.14 ± 0.71 | – | – | – |
| 911.38 ± 0.08 | 1.98 ± 0.09 | 6.68 ± 0.37 | 19.0 ± 1.7 | – | – | – |
| **916.09 ± 0.08**[f] | 2.16 ± 0.10 | 7.30 ± 0.40 | 21 ± 2 | 914.4 | 13 ± 2 | −2.79 |
| **939.31 ± 0.11**[f,j] | 0.40 ± 0.05 | 1.36 ± 0.17 | 3.86 ± 0.56 | – | – | – |
| **944.41 ± 0.15**[f] | 0.52 ± 0.05 | 1.76 ± 0.19 | 5.01 ± 0.65 | – | – | – |
| 946.67 ± 0.06 | 2.11 ± 0.11 | 7.11 ± 0.44 | 20 ± 2 | 947.0 ± 0.6[e] | 5.3 ± 0.8 | 4.41 |
| **954.68 ± 0.08**[f] | 0.91 ± 0.08 | 3.06 ± 0.29 | 8.72 ± 1.02 | – | – | – |
| 965.64 ± 0.16[d] | 0.22 ± 0.04 | 0.76 ± 0.14 | 2.15 ± 0.43 | – | – | – |
| **968.80 ± 0.13**[e,f] | 0.42 ± 0.06 | 1.42 ± 0.19 | 4.03 ± 0.62 | – | – | – |
| **974.49 ± 0.06**[f] | 2.42 ± 0.10 | 8.16 ± 0.42 | 23 ± 2 | 975.8 ± 1.0 | 4.5 ± 1.0 | 3.38 |
| **990.87 ± 0.07**[f] | 0.95 ± 0.06 | 3.20 ± 0.22 | 9.12 ± 0.90 | 991.4 ± 0.8 | 4.1 ± 0.8 | −1.08 |
| **1005.82 ± 0.10**[f] | 0.72 ± 0.05 | 2.42 ± 0.19 | 6.89 ± 0.74 | – | – | – |
| **1018.64 ± 0.07**[f] | 1.71 ± 0.10 | 5.77 ± 0.40 | 16.4 ± 1.6 | 1019.0 ± 0.8 | 6 ± 2 | −0.11 |
| **1025.40 ± 0.19**[f,i] | 0.26 ± 0.04 | 0.88 ± 0.15 | 2.52 ± 0.45 | – | – | – |
| **1034.43 ± 0.12**[f,j] | 1.44 ± 0.07 | 4.85 ± 0.29 | 13.8 ± 1.3 | 1035.2 ± 1.5 | 6 ± 2 | −0.57 |
| **1048.82 ± 0.10**[f] | 1.32 ± 0.10 | 4.46 ± 0.35 | 12.7 ± 1.4 | – | – | – |
| **1055.16 ± 0.10**[f] | 0.59 ± 0.06 | 1.98 ± 0.23 | 5.62 ± 0.76 | – | – | – |
| **1063.30 ± 0.06**[f] | 1.60 ± 0.13 | 5.40 ± 0.46 | 15.4 ± 1.7 | 1063.7 ± 0.8 | 5.9 ± 1.5 | −0.32 |
| **1068.07 ± 0.18**[f] | 0.27 ± 0.04 | 0.91 ± 0.15 | 2.59 ± 0.48 | – | – | – |
| **1072.86 ± 0.09**[f] | 0.78 ± 0.05 | 2.62 ± 0.18 | 7.47 ± 0.75 | – | – | – |
| **1085.49 ± 0.26**[f] | 0.31 ± 0.08 | 1.04 ± 0.29 | 2.96 ± 0.84 | – | – | – |
| **1092.27 ± 0.17**[f] | 0.74 ± 0.13 | 2.49 ± 0.43 | 7.08 ± 1.32 | – | – | – |
| **1094.58 ± 0.13**[f] | 1.39 ± 0.20 | 4.69 ± 0.69 | 13.4 ± 2.2 | 1094.1 ± 0.8[e] | 6 ± 2 | 0.59 |
| **1111.13 ± 0.19**[f,i] | 0.16 ± 0.03 | 0.54 ± 0.09 | 1.52 ± 0.27 | – | – | – |
| **1114.82 ± 0.16**[d,f,i] | 0.20 ± 0.04 | 0.68 ± 0.13 | 1.93 ± 0.41 | – | – | – |
| **1119.46 ± 0.28**[f] | 0.14 ± 0.04 | 0.48 ± 0.12 | 1.36 ± 0.36 | – | – | – |
| **1131.10 ± 0.12**[f,i,j] | 0.21 ± 0.03 | 0.72 ± 0.11 | 2.04 ± 0.35 | – | – | – |
| **1134.65 ± 0.14**[f] | 0.58 ± 0.07 | 1.97 ± 0.24 | 5.62 ± 0.79 | 1133.4 ± 1.5 | 2.8 ± 1.0 | −0.80 |
| **1147.96 ± 0.12**[f] | 0.43 ± 0.05 | 1.44 ± 0.18 | 4.10 ± 0.58 | – | – | – |
| **1156.25 ± 0.11**[f] | 0.55 ± 0.05 | 1.87 ± 0.19 | 5.31 ± 0.67 | 1156.9 ± 1.5 | 2.3 ± 0.9 | −0.47 |
| **1168.89 ± 0.09**[f,j] | 0.83 ± 0.06 | 2.79 ± 0.23 | 7.93 ± 0.86 | – | – | – |
| **1173.25 ± 0.09**[f] | 1.11 ± 0.09 | 3.73 ± 0.32 | 10.6 ± 1.2 | – | – | – |

**Table 2** (continued)

| This work | | | | From Demidov Atlas [26] | | *R* |
|---|---|---|---|---|---|---|
| $E_\gamma$ (keV) | $P_{E\gamma}(90°)/(\varepsilon_{E\gamma}{\cdot}f_{E\gamma})\times10^{-8}$ (count) | $I_R$(relative) (%) | $<\sigma_{E\gamma}(90°)>$ (mb) | $E_\gamma$ (keV) | $I_R$(relative) (%) | |
| **1178.78 ± 0.13**[d,f] | 0.72 ± 0.08 | 2.44 ± 0.29 | 6.95 ± 0.96 | – | – | – |
| **1190.69 ± 0.22**[f] | 0.38 ± 0.05 | 1.30 ± 0.18 | 3.69 ± 0.59 | – | – | – |
| **1193.60 ± 0.18**[f] | 0.65 ± 0.07 | 2.20 ± 0.24 | 6.26 ± 0.81 | – | – | – |
| **1196.05 ± 0.14**[f] | 0.59 ± 0.06 | 1.98 ± 0.21 | 5.63 ± 0.73 | 1195.1 ± 1.0[e] | 4.1 ± 0.8 | 0.10 |
| **1232.24 ± 0.18**[f] | 0.67 ± 0.10 | 2.27 ± 0.35 | 6.47 ± 1.10 | – | – | – |
| **1243.14 ± 0.32**[f] | 0.51 ± 0.09 | 1.74 ± 0.33 | 4.94 ± 0.99 | – | – | – |
| **1248.06 ± 0.24**[f] | 0.42 ± 0.13 | 1.43 ± 0.43 | 4.06 ± 1.25 | – | – | – |
| **1253.82 ± 0.10**[f,k] | 1.17 ± 0.09 | 3.95 ± 0.34 | 11.3 ± 1.3 | 1255.9 ± 1.1 | 4.7 ± 1.0 | −0.71 |
| **1269.04 ± 0.13**[f] | 0.38 ± 0.05 | 1.28 ± 0.18 | 3.64 ± 0.58 | – | – | – |
| **1273.60 ± 0.28**[f] | 0.36 ± 0.06 | 1.23 ± 0.21 | 3.50 ± 0.64 | – | – | – |
| **1276.05 ± 0.12**[d,f] | 1.10 ± 0.10 | 3.70 ± 0.35 | 10.5 ± 1.2 | 1276.7 ± 1.0[e] | 3.4 ± 0.9 | 1.66 |
| **1279.51 ± 0.27**[f] | 0.28 ± 0.05 | 0.94 ± 0.17 | 2.68 ± 0.51 | – | – | – |
| **1288.19 ± 0.12**[f] | 0.64 ± 0.06 | 2.16 ± 0.21 | 6.16 ± 0.74 | – | – | – |
| **1306.29 ± 0.24**[f] | 0.44 ± 0.06 | 1.49 ± 0.20 | 4.24 ± 0.65 | – | – | – |
| **1310.03 ± 0.13**[f] | 0.80 ± 0.06 | 2.71 ± 0.22 | 7.72 ± 0.83 | – | – | – |
| **1316.99 ± 0.12**[f] | 0.73 ± 0.05 | 2.45 ± 0.20 | 6.99 ± 0.75 | – | – | – |
| **1334.54 ± 0.17**[f] | 0.71 ± 0.07 | 2.40 ± 0.25 | 6.83 ± 0.86 | – | – | – |
| **1374.50 ± 0.12**[f,j] | 0.55 ± 0.04 | 1.84 ± 0.15 | 5.25 ± 0.57 | – | – | – |
| **1381.52 ± 0.16**[f] | 0.54 ± 0.05 | 1.82 ± 0.17 | 5.18 ± 0.62 | – | – | – |
| **1384.92 ± 0.21**[f] | 0.33 ± 0.04 | 1.11 ± 0.14 | 3.16 ± 0.46 | – | – | – |
| **1425.35 ± 0.30**[f] | 0.18 ± 0.04 | 0.62 ± 0.13 | 1.76 ± 0.40 | – | – | – |
| **1442.88 ± 0.12**[f] | 0.40 ± 0.03 | 1.36 ± 0.10 | 3.88 ± 0.39 | – | – | – |
| **1474.52 ± 0.43**[f] | 0.34 ± 0.08 | 1.15 ± 0.26 | 3.27 ± 0.77 | – | – | – |
| **1478.87 ± 0.32**[f,i] | 0.31 ± 0.06 | 1.05 ± 0.19 | 2.98 ± 0.58 | – | – | – |
| **1534.73 ± 0.27**[f,i] | 0.15 ± 0.03 | 0.52 ± 0.10 | 1.47 ± 0.31 | – | – | – |
| **1548.01 ± 0.16**[f] | 0.10 ± 0.02 | 0.35 ± 0.06 | 0.98 ± 0.20 | – | – | – |
| **1578.61 ± 0.21**[f] | 0.21 ± 0.04 | 0.71 ± 0.12 | 2.03 ± 0.37 | – | – | – |
| **2483.50 ± 0.54**[f,i] | 0.19 ± 0.05 | 0.63 ± 0.15 | 1.80 ± 0.46 | – | – | – |
| **3333.07 ± 0.43**[f,i] | 0.16 ± 0.04 | 0.55 ± 0.13 | 1.57 ± 0.39 | – | – | – |
| **3353.65 ± 0.58**[f,i] | 0.09 ± 0.03 | 0.30 ± 0.11 | 0.86 ± 0.32 | – | – | – |

$E_\gamma$ denotes the gamma-ray energy, $P_{E\gamma}(90°)/(\varepsilon_{E\gamma}{\cdot}f_{E\gamma})$ the net counts in the gamma-ray peak divided by the full-energy-peak (FEP) efficiency and the gamma-ray self-absorption factor, $I_R$ the relative gamma-ray intensity and $<\sigma_{E\gamma}(90°)>$ the fission-neutron spectrum-averaged partial cross section for gamma-ray production at an angle of 90° between neutron beam and detector determined with Eq. (1). *R* represents the residual calculated by means of Eq. (7). Gamma lines written in bold are not yet listed in [29, 30]

[a]Reaction threshold for inelastic scattering is 58.36 keV[41, 51]

[b]Emitted from same excited level as 317.01 keV, corrected for strong background interference

[c]Corrected for interference from the $^{35}$Cl(n,n′γ)$^{35}$Cl reaction; $<\sigma_{E\gamma}(90°)> = (32 \pm 3)$ mb [16] yields a contribution to the total counts of 1.7%

[d]Corrected for contribution of neutron capture interference from the $^{159}$Tb(n,γ)$^{160}$Tb reaction

[e]Unresolved doublet, intensity of 183.06 & 184.48 keV, 303.40 & 306.82 keV, 944.41 & 946.67 keV, 1092.27 & 1094.58 keV, 1193.60 & 1196.05 keV, 1273.60 & 1276.05 keV

[f]Not listed in [29, 30], any other reaction than (n,n′γ) excluded

[g]Probably interchanged intensities between 272.9 and 274.8 keV

[h]Intensity of 615.4 & 617.5 keV

[i]Tentative and uncertain suggestion

[j]Corrected for contribution of neutron capture interference from the $^{35}$Cl(n,γ)$^{36}$Cl reaction with data from[34]

[k]Corrected for interference with SE from the 1763-keV line of $^{35}$Cl; 23.4% contribution to the net counts

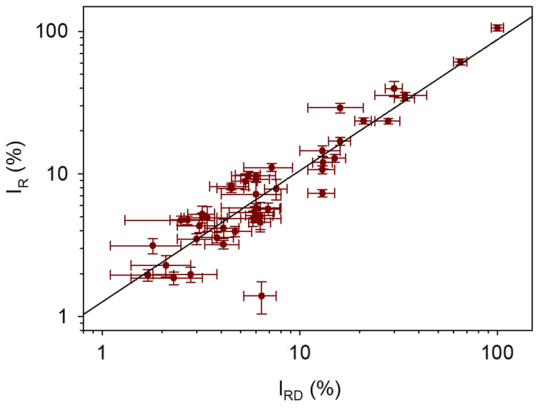


**Fig. 6** Correlation between the relative intensities $I_R$ of the prompt gamma rays issued from fast-neutron inelastic scattering (n,n′γ) reactions on terbium measured in this work and the relative intensities $I_{RD}$ listed in the Demidov Atlas [26]. The fit of the data according to Eq. (6) is shown by the solid line

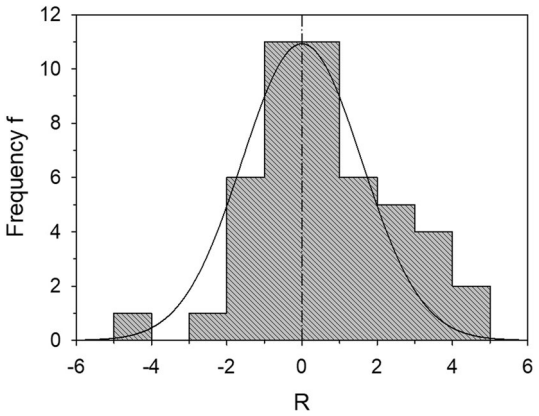


**Fig. 7** Histogram plot of the residuals $R$, calculated with Eq. (7) in units of standard deviation [$\sigma$], demonstrating the agreement between the relative intensities of prompt gamma rays from the $^{159}$Tb(n,n′γ)$^{159}$Tb reaction derived in this work with the data listed in [26]. The data was fitted with a Gaussian, which is shown by the solid line

$$R = \frac{I_R - I_{RD}}{\sqrt{\left(s_{I_R}\right)^2 + \left(s_{I_{RD}}\right)^2}} \tag{7}$$

The data is fitted with a Gaussian and it agrees at the $1.6\sigma$ level with the Gaussian centroid being aligned at $R = 0.00 \pm 0.26$, indicating no relevant systematic effect. One should be aware, however, that Demidov et al. mention the presence of capture lines in their spectra, but no reliable information is given according to their treatment of interferences.

The partial cross sections for the production of identified gamma-rays, averaged over the fast-neutron spectrum and calculated by means of Eq. (1) with a flux of $(1.13 \pm 0.04) \times 10^8$ cm$^{-2}$ s$^{-1}$, are given in column 4 of Table 2.

## Prompt gamma rays of oxygen and chlorine

The prompt gamma lines induced by interaction of fast neutrons on oxygen and chlorine were also analyzed and the corresponding partial cross sections determined by means of Eq. (1). The values obtained for the 1981-keV line from $^{18}$O(n,n′γ)$^{18}$O, $213 \pm 40$ mb, and for the 6129-keV line from $^{16}$O(n,n′γ)$^{16}$O, $2.22 \pm 0.31$ mb, agree well with the values achieved in our work on $CaCO_3$ [15], i.e. $201 \pm 28$ mb and $2.20 \pm 0.37$ mb, respectively. The 1981-keV line was corrected for the interference with the DE from the 3002-keV line of $^{35}$Cl, with a contribution to the net counts of $(39.4 \pm 6.6)\%$.

In the case of chlorine, 28 lines were observed, 15 associated to $^{35}$Cl(n,n′γ)$^{35}$Cl, 9 to $^{37}$Cl(n,n′γ)$^{37}$Cl and 4 to $^{35}$Cl(n,pγ)$^{35}$S. The 78.0-keV line from $^{35}$Cl(n,αγ)$^{32}$P observed in [16] was not considered uniquely due to the strong interference of the 79-keV line from the $^{159}$Tb(n,n′γ)$^{159}$Tb reaction. The ratios of measured partial cross sections to the values obtained in our work on $CeCl_3$ [16] are shown in Fig. 8. Taking the corresponding uncertainties into account, the data of both measurements is observed to agree well with each other.

## Detection limit

The smallest amount of a pure element that is related to the measurement of a net signal above the background with a certain standard deviation $\sigma$ obtained by the irradiation over a certain time corresponds to the detection limit (DL).

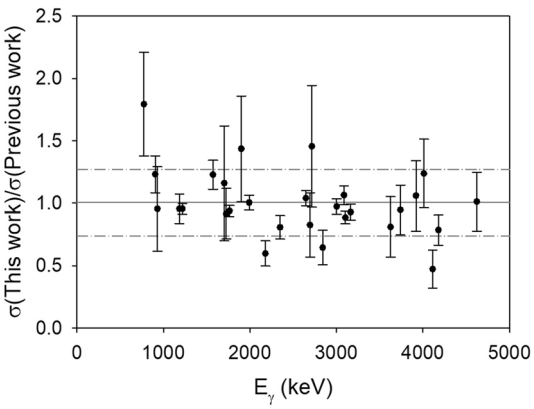


**Fig. 8** Ratio of gamma-ray production cross sections $<\sigma_{E\gamma}(90°)>$ in mb for chlorine lines from (n,n′γ) and (n,pγ) reactions obtained in this work compared to these obtained in our previous work [16]. The solid line represents the mean value of the ratios, i.e. $1.00 \pm 0.27$, while the dash-dotted lines represent the error margins corresponding to one standard deviation

Neglecting neutron self-shielding and gamma-ray self-absorption, i.e. $f_n = 1$ and $f_{E\gamma} = 1$, respectively, the value of the DL can be determined with Eq. (1) from the minimum peak area $P_{E\gamma}(c)$ that could be expressed according to [55] as:

$$P_{E\gamma}(c) = \frac{\sqrt{2 \cdot B_{E\gamma}}}{c} \quad (8)$$

where $B_{E\gamma}$ represents the area of the background below the gamma line of interest and $c$ equals a predefined value for the relative uncertainty of the peak area.

The DL of terbium was calculated for the most intense gamma line by means of Eqs. (1) and (8) assuming a counting live time of 12 h. The HYPERMET-PC [28] software was used to determine the value of $B_{E\gamma}$ from the beam background. For a peak area uncertainty of 50%, i.e. a value of $c = 0.5$ in Eq. (8), the smallest amount of pure element that can be detected is 1 mg for terbium ($^{159}$Tb, $E_\gamma = 57.9$ keV, $< \sigma_{E\gamma}(90°) > = 445$ mb).

## Conclusions

The emission of prompt gamma rays in terbium induced by (n,n′γ) reactions was examined with the FaNGaS instrument by irradiating a $TbCl_3 \cdot 6H_2O$ sample with fission neutrons. To correct for interferences of radiative-capture lines of terbium and chlorine the thermal and epithermal neutron flux within the sample were determined from the interference-free (n,γ)-lines of terbium and chlorine. Simulations performed with the MCNP code show a significant increase of the neutron flux below a neutron energy of 1 eV, which is related to the moderation of neutrons by water of crystallization. Comparison of the experimental and simulated sample-flux values indicates an increase of the incident thermal and epithermal neutron flux by a factor of 4 and 2, respectively; the fast-neutron flux being unchanged. We associate the increase of the flux in the thermal and epithermal regions to the MLC made of materials enabling neutron moderation.

In total, we identified 124 prompt gamma lines from the $^{159}$Tb(n,n′γ)$^{159}$Tb reaction. Relative intensities as well as fast-neutron spectrum-averaged partial gamma-ray production cross sections were measured. Compared to the work of Demidov et al. [26] we were able to detect 76 additional gamma lines, which is mainly attributed to the better energy resolution of our detector and a higher mean neutron energy. Since the majority of observed lines is unreported in [29, 30], we consider this work as an important contribution to the expansion of terbium level and decay schemes. Our relative intensities are in reasonable agreement (1.6$\sigma$ level) with the values listed in [26]. The detection limit of terbium was determined as 1 mg assuming a counting time of 12 h. Furthermore, the partial production cross sections for prompt gamma lines of oxygen and chlorine were found to agree well with the values from previous works [15, 16].

**Funding** Open Access funding enabled and organized by Projekt DEAL.

## Declarations

**Conflict of interest** The authors have no competing interests to declare that are relevant to the content of this article. The 7th author Zsolt Révay is an editor of this journal. Therefore, he did not take part in the review process in any capacity and the submission was handled by a different member of the editorial board.



## References

1. Molnár GL (2004) Handbook of prompt gamma activation analysis with neutron beams. Kluwer Academic Publishers ISBN 1–4020–1304–3
2. Paul RL, Lindstrom RM (2000) Prompt gamma-ray activation analysis: fundamentals and applications. J Radioanal Nucl Chem 243:181–189
3. Shaw DM (1998) Prompt gamma neutron activation analysis. J Neutron Res 7:181–194
4. Kudejova P, Materna Th, Jolie J, Türler A, Wilk P, Baechler S, Zs K, Zs R, Belgya T (2005) On the construction of a new instrument for cold-neutron prompt gamma-ray activation analysis at the FRM-II. J Radioanal Nucl Chem 265:221–227
5. Kudejova P, Meierhofer G, Zeitelhack K, Jolie J, Schulze R, Türler A, Materna Th (2008) The new PGAA and PGAI facility at the research reactor FRM II in Garching near munich. J Radioanal Nucl Chem 278:691–695
6. Cancella L, Kudejova P, Schulze R, Türler A, Jolie J (2011) Characterisation and optimization of the new Prompt Gamma-ray Activation Analysis (PGAA) facility at FRM II. Nucl Instrum Methods A 636:108–113
7. Zs R, Kudejova P, Kleszcz K, Söllradl S, Genreith C (2015) In-beam activation analysis facility at MLZ, Garching. Nucl Instrum Methods A 799:114–123
8. Kluge E, Stieghorst C, Wagner FE, Gebhard R, Zs R, Jolie J (2018) Archaeometry at the PGAA facility of MLZ—Prompt gamma-ray neutron activation analysis and neutron tomography. J Archaeol Sci Rep 20:303–306
9. Rossbach M, Genreith C, Randriamalala T, Mauerhofer E, Zs R, Kudejova P, Söllradl S, Belgya T, Szentmiklosi L, Firestone RB, Hurst AM, Bernstein L, Sleaford B, Escher JE (2015) TANDEM: a mutual cooperation effort for transactinide nuclear data evaluation and measurement. J Radioanal Nucl Chem 304:1359–1363

10. Randriamalala TH, Rossbach M, Mauerhofer E, Zs R, Söllradl S, Wagner FM (2016) FaNGaS: A new instrument for (n, n´γ) reaction measurements at FRM II. Nucl Instrum Methods A 806:370–377
11. Hable A, Ramsl C, Jericha E, Böck H, Randriamalala TH, Rossbach M (2017) FaNGaS: Determination of integral fast fission cross sections (n, f) of $^{23}$8U, $^{23}$7Np, and $^{24}$2Pu in a directed fission neutron beam at FRM II. Garching, J Radioanal Nucl Chem. https://doi.org/10.1007/s10967-017-5512-7
12. Ilic Z, Mauerhofer E, Stieghorst C, Zs R, Rossbach M, Randriamalala TH, Brückel T (2020) Prompt gamma rays induced by inelastic scattering of fission neutrons on iron. J Radioanal Nucl Chem 325:641–645
13. Mauerhofer E, Ilic Z, Stieghorst C, Zs R, Rossbach M, Li J, Randriamalala TH, Brückel T (2021) Prompt and delayed gamma rays induced by epithermal and fast neutrons with indium. J Radioanal Nucl Chem 331:535–546
14. Mauerhofer E, Ilic Z, Stieghorst C, Zs R, Vezhlev E, Ophoven N, Randriamalala TH, Brückel T (2022) Prompt gamma rays from fast neutron inelastic scattering on aluminum, titanium and copper. J Radioanal Nucl Chem 331:3987–4000
15. Ophoven N, Ilic Z, Mauerhofer E, Randriamalala TH, Vezhlev E, Stieghorst C, Zs R, Brückel T, Jolie J, Strub E (2022) Fast neutron induced gamma rays from (n, n'), (n, p) and (n, α) reactions on CaCO3. J Radioanal Nucl Chem 331:5729–5740
16. Ophoven N, Ilic Z, Mauerhofer E, Randriamalala TH, Vezhlev E, Stieghorst C, Zs R, Brückel T, Jolie J, Strub E (2023) Prompt gamma rays from fast neutron induced reactions on cerium and chlorine. J Radioanal Nucl Chem 332:3133–3145
17. Schrader CD, Stinner RJ (1961) Remote analysis of surfaces by neutron-gamma-ray inelastic scattering techniques. J Geophys Res 66:1951–1956
18. Jiggins AH, Habbani FI (1976) Prompt gamma-ray analysis using 3.29 MeV neutron inelastic scattering. Int J Appl Radiat Isot 27:689–693
19. Yates SW, Filo AJ, Cheng CY, Coope DF (1978) Elemental analysis by gamma detection following inelastic neutron scattering. J Radioanal Nucl Chem 46:343–355
20. Sowerby BD (1979) Elemental analysis by neutron inelastic scatter gamma rays with a radioisotope source. Nucl Instrum Methods 166:571–579
21. Ahmed MR, Demidov AM, Al-Najjar SA, Al-Amili MA (1974) Use of spectroscopy of gamma-radiation from the inelastic scattering of reactor fast neutrons for elemental analysis. J Radioanal Nucl Chem 23:199–203
22. Wagner F, Kneschaurek P, Kastenmüller A, Loeper-Kabasakal B, Kampfer S, Breitkreutz H, Waschkowski W, Molls M, Petry W (2009) The munich fission neutron therapy facility MEDAPP at the research reactor FRM II. Strahlenther Onkol. https://doi.org/10.1007/s00066-008-1878-3
23. Bernstein L, Brown D, Basunia S, Hurst A, Kawano T, Kelley J, Kondev F, McCutchan E, Nesaraja C, Slaybaugh R, Sonzogni A, (2015) Nuclear data needs and capabilities for applications, White paper LLNL Report LLNL-CONF-676585
24. Romano C, Ault T, Bernstein L, Bahran R, Talou P, Quiter B, Pozzi S, Devlin M, Burke J, Bredeweg T, McCutchan E, Stave S, Bailey T, Hogle S, Chapman C, Hurst A, Nelson N, Tovesson F, Hornback D, (2018) Proceedings of the nuclear data roadmapping and enhancement workshop (NDREW) for nonproliferation, In: White paper ORNL/LTR-2018/510, https://www.nndc.bnl.gov/nndcscr/documents/ndrew/NDREWProc_FINAL.pdf
25. Bernstein L, Romano C, Brown D, Casperson R, Descalle MA, Devlin M, Pickett C, Rearden B, Vermeulen C, (2019) Final report for the workshop for applied nuclear data activities (WANDA), White Paper LLNL-PROC-769849
26. Demidov A, Govor L, Cherepantsev M, Ahmed S, Al-Najjar M, Al-Amili N, Al-Assafi N, Rammo N (1978) Atlas of gamma-ray spectra from the inelastic scattering of reactor fast neutrons. Atomizdat, Moscow
27. Hurst AM, Bernstein LA, Kawano T, Lewis AM, Song K (2021) The Baghdad Atlas: a relational database of inelastic neutron scattering (n, n´γ) data. Nucl Instrum Meth A 995:165095
28. Zs R, Belgya T, Molnár GL (2005) Application of Hypermet-PC in PGAA. J Radioanal Nucl Chem 265:261–265
29. NuDat 3.0 National Nuclear Data Center, Brookhaven National Laboratory https://www.nndc.bnl.gov/nudat3/
30. Reich CW (2012) Nuclear data sheets for A= 159. Nucl Data Sheets 113:157–363
31. Chen J, Cameron J, Singh B (2011) Nuclear data Sheets for A= 35. Nucl Data Sheets 112:2715–2850
32. Cameron J, Chen J, Singh B, Nica N (2012) Nuclear Data Sheets for A= 37. Nucl Data Sheets 113:365–514
33. Ouellet C, Singh B (2011) Nuclear data sheets for A= 32. Nucl Data Sheets 112:2199–2355
34. Zs R, Firestone RB, Belgya T, Molnár, (2004) Prompt Gamma-Ray Spectrum. In: Molnár GL (ed) Handbook of prompt gamma activation analysis with neutron beams. Kluwer Academic Publishers, Dordrecht/Boston/New York, pp 173–364
35. Reilly D et al., (1991) Passive nondestructive assay of nuclear materials https://www.nrc.gov/docs/ML0914/ML091470585.pdf
36. NIST XCOM: Photons Cross Sections Database, National Institute of Standards and Technology https://physics.nist.gov/PhysRefData/Xcom/html/xcom1.html
37. Berger MJ, Hubbell JH, Seltzer S, Chang J, Coursey JS, Sukumar R, Zucker DS (2009) XCOM: Photon cross sections database. NIST Stand Ref Database 8:87–3597
38. MacFarlane RE, Kahler AC (2010) Methods for processing ENDF/B-VII with NJOY. Nucl Data Sheets 111:2739–2890
39. MacFarlane R, Muir DW, Boicourt RM, Kahler AC, Conlin JL (2017) The NJOY nuclear data processing system. Version. https://doi.org/10.2172/1338791
40. Brown DA et al (2018) ENDF/B-VIII.0: The 8th major release of the nuclear reaction data library with CIELO-project cross sections, New standards and thermal scattering data. Nucl Data Sheets 148:1–142
41. Shibata K, Iwamoto O, Nakagawa T, Iwamoto N, Ichihara A, Kunieda S, Chiba S, Furutaka K, Otuka N, Ohsawa T, Murata T, Matsunobu H, Zukeran A, Kamada S, Katakura J (2010) JENDL-4.0: A new library for nuclear science and engineering. J Nucl Sci Technol 48(1):1–30
42. Plompen AJM et al (2020) The joint evaluated fission and fusion nuclear data library, JEFF-3.3. Eur Phys J A. https://doi.org/10.1140/epja/s10050-020-00141-9
43. Kahler AC et al. (2020) Multifaceted coded nuclear data libraries assemblage, verification and validation: TENDL-2019. Conference 2020 ANS Virtual Winter Meeting. https://doi.org/10.13182/T123-33321
44. OECD NEA Data Bank, (2020) JANIS Book of neutron-induced cross-sections https://www.oecd-nea.org/janis/book/book-neutron-2020-09.pdf
45. Initial MCNP6 Release overview MCNP6 version 1.0, Los Alamos National Laboratory report LA-UR-13–22934
46. Goorley T et al (2017) Initial MCNP6 release overview. Nucl Technol 180:298–315
47. Conlin JL, Haeck W, Neudecker D, Parsons DK, White MC (2018) Release of ENDF/B-VIII.0-Based ACE Data Files, Los Alamos National Laboratory report LA-UR-18–24034 https://nucleardata.lanl.gov/files/la-ur-18-24034.pdf
48. Szentmiklósi L, Kis Z, Maróti B, Horváth LZ (2021) Correction for neutron self-shielding and gamma-ray at self-absorption

in prompt-gamma activation analysis for large and irregularly shaped samples. J Anal At Spectrom 36:103–110
49. Romero-Barrientos J, Molina F, Aguilera P, Arellano HF (2016) Calculation of self-shielding factor for neutron activation experiments using GEANT4 and MCNP. AIP Conf Proc 1753:080018
50. Molina F, Aguilera P, Romero-Barrientos J, Arellano HF, Agramunt J, Medel J, Morales JR, Zambra M (2017) Energy distribution of the neutron flux measurements at the Chilean reactor RECH-1 using multi-foil neutron activation and the expectation maximization unfolding algorithm. Appl Radiat Isot 129:28–34
51. Nuclear Data Center, (1996) Japan atomic energy agency, tables of nuclear data https://wwwndc.jaea.go.jp/jendl/j40/j40.html
52. Chu SYF, Ekström LP, Firestone RB, WWW Table of radioactive isotopes, database version 1999–02–28. http://nucleardata.nuclear.lu.se/toi/
53. Barzilov A, Womble P (2014) Study of Doppler broadening of gamma-ray spectra in 14-MeV neutron activation analysis. J Radioanal Nucl Chem 301:811–819
54. Catz AL, Amiel S (1967) Study of lifetimes of nuclear levels by Doppler broadening attenuation using a (Ge)Li gamma-ray spectrometer. Nucl Phys A 92:222–232
55. Zs R (2009) Determining elemental composition using prompt γ activation analysis. Anal Chem. https://doi.org/10.1021/ac9011705